Applied Catalysis B: Environmental 323 (2023) 122134

Contents lists available at ScienceDirect

Applied Catalysis B: Environmental

journal homepage: www.elsevier.com/locate/apcatb

An unprecedented 2-fold interpenetrated ***lvt*** open framework built from Zn_6 ring seamed trivacant polyoxotungstates used for photocatalytic synthesis of pyridine derivatives

Xianqiang Huang [a,*,1], Sen Liu [a,1], Gang Liu [a], Yiwei Tao [a], Chenran Wang [a], Yalin Zhang [a], Zhen Li [a], Huaiwei Wang [a], Zhen Zhou [c,*], Guodong Shen [a], Zechun Xue [a], Di Sun [b,*]

[a] *Shandong Provincial Key Laboratory of Chemical Energy Storage and Novel Cell Technology, School of Chemistry & Chemical Engineering, Liaocheng University, Liaocheng 252059, PR China*

[b] *School of Chemistry and Chemical Engineering, State Key Laboratory of Crystal Materials, Shandong University, Ji'nan 250100, PR China*

[c] *School of Chemistry and Chemical Engineering, Shandong University of Technology, Zibo 255000, PR China*

ARTICLE INFO

Keywords:
Polyoxometalates
Polyoxotungstates
Crystal structure
Photocatalysis
Pyridines

ABSTRACT

Solar-driven straightforward one-step synthesis of pyridine derivatives in the absence of photosensitizer is of considerable interest but greatly challenging in synthetic and medicinal chemistry. Herein, an unprecedented 2-fold interpenetrated ***lvt*** polyoxometalate-based open framework (POM-OF), **LCU-22** ($[Zn(1\text{-ipIM})_3]_2[Zn_6(AsW_9O_{33})_2(1\text{-ipIM})_6]\cdot 2(1\text{-HipIM})$, 1-ipIM = 1-isopropyl imidazole) has been synthesized in gram-scale quantities using one-pot reaction and structurally characterized by X-ray crystallography. The cluster node in **LCU-22** is a Zn_6 ring seamed trivacant polyoxotungstate cluster ($[Zn_6(AsW_9O_{33})_2]$), which is quadruply extended by $[Zn(1\text{-ipIM})_3]^{2+}$ units to form the final 3D open framework. Remarkably, **LCU-22** is highly stable over wide pH range and in various solvents, and dramatically boosted the white light-powered heterogeneous photocatalysis for synthesis of pyridine derivatives in good yields after three times recycles utilization. This work not only builds a novel POM-OF but also underscores the unique advantages of transition metal cluster substituted polyoxotungstates frameworks used for selective photocatalytic formation of value-added organic molecules.

1. Introduction

The development of high efficiency, green energy sources and eco-friendly organic conversion approach has become an imperative task in the field of synthetic chemistry [1,2]. As a promising green strategy, the visible-light photocatalytic technology could utilize the sunlight to effectively transform the cheap and readily available organic substrates to high value-added functional chemicals [3–6]. Therefore, visible-light photocatalytic reaction is considered to be one of the most effective and powerful ways for organic conversion and has recently witnessed unprecedented advancements [7–10].

Among the numerous organic reactions, synthesis of pyridines is considered a remarkable and substantial organic transformation in the field of pharmaceuticals, polymers, and agrochemicals industries [11–16]. Generally, 1,4-dihydropyridines were classically prepared by one-pot reaction of β-ketoesters, aldehydes and ammonia source, and their oxidation products pyridines could be achieved via the oxidation of above-obtained dihydropyridine compounds [17,18]. However, these protocols are associated with inevitable drawbacks including the use of stoichiometric costly oxidant, the two-step reaction process and excess additives, etc. To our best knowledge, the formation of 1,4-dihydropyridines and pyridines in a one-step fashion from aldehydes, β-ketoesters and ammonia under photo-assisted conditions is still greatly challenging but highly desirable [19]. Thus, it is urgent need to develop efficient photocatalysts for achieving these functionalized pyridines.

As an alternative, polyoxometalates (POMs) are a class of polynuclear, early transition-metal nanoclusters with a great potential in various fields, especially, catalysis [20], biology [21], energy [22], and so on. Among POMs, the trivacant Keggin fragments could act as functionalized ligands and coordinate with transition metal cations to form various sandwich-type structures [23]. Nevertheless, most transition metal modified sandwich-type POMs mainly focused on two to five

* Corresponding authors.
E-mail addresses: hxq@lcu.edu.cn (X. Huang), zhouzhen@sdut.edu.cn (Z. Zhou), dsun@sdu.edu.cn (D. Sun).

[1] These authors contributed equally to this work.

https://doi.org/10.1016/j.apcatb.2022.122134
Received 7 September 2022; Received in revised form 27 October 2022; Accepted 30 October 2022
Available online 1 November 2022
0926-3373/© 2022 Elsevier B.V. All rights reserved.

transition metals in the linking belt, and only a few hexa-substituted analogues have been reported. For instance, Yang et al. synthesized three $M_4(XW_9O_{34})_2$ (M = Cu, Zn; X = Si, P) clusters with reversible water-sorption capabilities [24]. Toshihiro's group presented four $(MCl)_6(XW_9O_{33})$ (M = Cu, Mn; X = As, Sb) clusters with interesting magnetic behavior [25,26]. To the best of our knowledge, the most investigations based on the hexa-substituted transition metals in the linking belt of sandwich-type POMs are mainly focused on silicotungstates and germanotungstates. However, the reported results on arsenotungstates (ATs) are relatively limited although ATs are an important subfamily bearing enormous diversity of properties and structures in POMs chemistry. Moreover, the most cases only represented the hexa-substituted sandwiched $M_6(AsW_9O_{33})_2$ units, which are hardly extended to 3D POM-OFs [27], not matter to say, the ATs-based POM-OFs have become the most promising photocatalyst candidates owing to their proper energy levels of the frontline molecular orbitals. Hence, the one-step photosynthesis of pyridines catalyzed by the ATs-based POM-OF is eagerly desirable.

In this work, we demonstrated a novel 2-fold interpenetrated POM-OF (**LCU-22**) with a Zn_6 ring seamed trivacant polyoxotungstates as cluster node that was further linked by four $[Zn(1\text{-ipIM})_3]^{2+}$ units to 3D open framework. Importantly, the photocatalytic oxidation by **LCU-22** was further investigated under visible light irradiation ($\lambda > 390$ nm), which presented remarkable catalytic performance toward the one-pot synthesis of pyridine derivatives (yields up to 87 %) at room temperature. The recyclability experiments also confirmed that **LCU-22** possessed excellent reusability without the loss of its activities.

2. Experimental

2.1. Materials and characterization

Sodium tungstate dihydrate (Energy Chemical, 99 %), sodium arsenate (Chengdu Aikeda Chemical Reagent Company, 99 %), antimony trioxide (Chengdu Aikeda Chemical Reagent Company, 99 %), zinc chloride (Energy Chemical, 99 %), ammonium acetate (Tianjin Kemiou Reagent Co., LTD. Chemistry), 1-isopropyl imidazole (Aladdin Chemical, 99 %), methyl acetoacetate (Aladdin Chemical, 99 %), aromatic aldehydes (J&K Scientific Ltd. and Energy Chemical, 98 %). All chemical reagents and solvents used were purchased from commercial sources without further purification.

The Fourier transform infrared (FT-IR) spectrum of **LCU-22** was recorded on Nicolet 170 SXFT/IR spectrometer in the range 4000–400 cm^{-1}. Powder X-ray diffraction pattern (PXRD) data was obtained by using a Rigaku D/max-2550 diffractometer with Cu-Kα radiation. The elemental analyses were tested on Perkin-Elmer 240 C elemental analyzer. The GC analyses were performed on Shimadzu GC-2014 C with an FID detector equipped with a Wonda Cap Hp-5 Sil capillary column. The GC mass spectra (GC-MS) were recorded on Agilent 7890B-7000D. X-ray photoelectron spectroscopy (XPS) (Escalab Xi+, Thermo Fisher Scientific Pvt. Ltd., UK) photoelectron spectrometer with a monochromatized Al-Kα X-ray source was carried out to analyze before and after of the surface elements of **LCU-22**. Single X-ray diffraction (SXRD) data were performed on a Bruker-AXS CCD diffractometer equipped with a graphite-monochromated Mo-Kα radiation (λ = 0.71073 Å) at 298 K.

2.2. Synthesis of $[Zn(1\text{-ipIM})_3]_2[Zn_6(AsW_9O_{33})_2(1\text{-ipIM})_6]\cdot 2(1\text{-HipIM})$ (LCU-22)

$Na_2WO_4\cdot 2H_2O$ (0.04 g, 0.12 mmol) and $NaAsO_2$ (0.02 g, 0.12 mmol) were dissolved in 5 mL H_2O. $ZnCl_2\cdot 2H_2O$ (0.02 g, 0.15 mmol) and 1-ipIM (0.14 mL, 1.23 mmol) were dissolved in 5 mL H_2O, then the solution was added dropwise to the above mixture. The pH of the resulting mixture was adjusted to 6.5 by adding 4 M HCl, finally the solution was then sealed in a 15 mL Teflon reactor and heated at 160 °C for 3 days. White crystals suitable for X-ray diffraction were obtained. Yield: 52.4 %. Elemental analysis for $C_{42}H_{71}AsN_{14}O_{33}W_9Zn_4$: calc. (found) (%): C, 15.32 (15.29); H, 2.16 (2.18); N, 5.96 (5.93); As, 2.28 (2.29); W, 50.29 (50.27); Zn, 7.95 (7.93). FT-IR data (KBr pellet, cm^{-1}): 3442 (s), 3124 (s), 2977 (m), 1634 (v), 1522 (v), 1417 (v), 1373 (v), 1242 (v), 1114 (s), 1013 (s), 943 (s), 839 (s), 740 (s), 489 (s).

2.3. General procedure for photosynthesis of pyridines

In a 25 mL quartz glass tube, methyl acetoacetate (2 mmol), aromatic aldehydes (1 mmol), ammonium acetate (1 mmol), **LCU-22** (10 mg, 0.15 mol%) and methanol (2 mL) were successively added and the mixture was irradiated by visible-light irradiation (10 W white LEDs, $\lambda_p = \lambda \pm 10$ nm) and simultaneously magnetically stirred at 500 rpm at room temperature under molecular oxygen atmosphere (1 atm, balloon) in a Wattecs Parallel Photocatalytic Reactor (WP-TEC-1020HSL) for appropriate reaction time (monitored by GC). After the reactions were completed, the organic phases were analysed by GC and GC-MS, the isolated pyridine derivatives were further characterized by NMR.

2.4. Reuse experiment of LCU-22

The reuse experiment was carried out on the photocatalytic reaction of benzaldehyde, methyl acetoacetate and ammonium acetate. After the reaction was completed, the photocatalyst was separated by centrifugation, washed and soaked with absolute methanol (ca. 3 × 5 mL), and air-dried prior to being used for the reuse experiment. In addition, the retrieved catalyst could be reused for the photosynthesis of pyridine derivatives without an appreciable loss of its high catalytic performance.

2.5. X-ray crystallography

Crystal data for **LCU-22** were collected at 293 K on a Bruker Apex-II CCD diffractometer with graphite-monochromated Mo Kα radiation (the value of λ is 0.71073 Å). The SADABS scheme was used for routine Lorentz and polarization rectification. The structure of **LCU-22** was solved by direct methods using the SHELXS-97 software [28]. In the final refinement, the W and Zn atoms of **LCU-22** were anisotropically refined. Non-H atoms in the **LCU-22** were refined with anisotropic thermal parameters. The H atoms of the 1-ipIM were placed in calculated positions and then refined using a riding model. Crystallographic data and structure refinement parameters for **LCU-22** (CCDC 2164552) are given in Table S1. The selected bond lengths and angles are listed in Table S2.

3. Results and discussion

3.1. Synthesis and characterization of LCU-22

Following our previous work on the imidazole modified POMs [29], and aim to explore the controllable conditions toward the construction of the various POMs with potential catalytic applications, herein, we picked up the simple tungsten source Na_2WO_4 as the starting precursor to react with $ZnCl_2$ along with imidazole ligands and $NaAsO_2$ in an acidic system under hydrothermal conditions.

During the assembly process of **LCU-22**, several key synthetic factors, such as organic ligands, pH and different precursors of POMs need to be emphasized. Liquid imidazole derivatives as a kind of cheap and commercially available organic base and solvents have served as desired N-ligands to coordinate with the metal sites in the synthesis of functionalized POMs. Nevertheless, imidazole-decorated sandwich-type polyoxotungstates are still rare. In this work, 1-ipIM was certified as suitable imidazole substitutes to synthesize the imidazole functionalized sandwich-type polyoxotungstates. While the 1-mIM and 1-eIM were utilized as the ligands in the reaction instead of the 1-ipIM (1-mIM = 1-methylimidazole, 1-eIM = 1-ethylimidazole), the white milky

precipitates and white translucent solution were produced, respectively, indicating that 1-ipIM are essential for the formation of **LCU-22**. Besides, it is well known that pH value plays a crucial role in the formation of POMs; thus, **LCU-22** was synthesized controllably in a narrowed pH range of 6.0–6.8 and the needle-like single crystals suitable for X-ray diffraction were obtained at pH = 6.5. When pH value reached 3.2, the single crystals of $Na_{10}H_2W_{12}O_{42}{\cdot}23\ H_2O$ were achieved (Fig. S1). Additionally, the replacing $ZnCl_2$ with $CuCl_2$ or $NiCl_2$ would not promote the formation of crystalline Cu/Ni-containing polyoxotungstates under the same conditions. Furthermore, it was disappointed that no crystals were achieved when Na_2WO_4 was replaced with Na_2MoO_4.

Single crystal X-ray diffraction revealed that **LCU-22** was crystallized in a tetragonal space group $P4_2/n$ and composed of a decorated sandwich-like polyoxotungstate $[Zn_6(AsW_9O_{33})_2(1\text{-ipIM})_6]^{6-}$, two $[Zn(1\text{-ipIM})_3]^{2+}$ units and two lattice 1-HipIM as countercation. As shown in Fig. 1a, the $[Zn_6(AsW_9O_{33})_2(1\text{-ipIM})_6]^{6-}$ anion is constructed from two trivacant Keggin-type $[AsW_9O_{33}]^{9-}$ anions, each of which sandwiches a ring-like $[Zn_6(1\text{-ipIM})_6]^{12+}$ cluster in the middle (Fig. 1b), and also coordinates to four $[Zn(1\text{-ipIM})_3]^{2+}$ subunits by four terminal oxygen atoms from the side and the vertex (Fig. 1c). The whole structure is ca. 1.5 nm height, and contains a confined inner cavity where resides two AsO_3^{3-} heteroanions separating 5.323 Å based on the As···As interatomic distance. The bond lengths of As-O are ranging from 1.804(13) − 1.817(15) Å. The diameter of ring-like $[Zn_6(1\text{-ipIM})_6]^{12+}$ cluster in the middle is 6.183 Å. All Zn atoms in the Zn_6 ring (Zn1, Zn2 and Zn3) are coordinated by four terminal O atoms at trivacant region of $[AsW_9O_{33}]^{9-}$ anions and one N atom from one 1-ipIM ligand, resulting in a distorted tetragonal pyramid geometry (Fig. S2a), whereas another Zn atom (Zn4) outside of the central $[Zn_6(AsW_9O_{33})_2(1\text{-ipIM})_6]^{6-}$ cluster is bonded by two terminal oxygen atoms and three N atoms from three 1-ipIM ligands to form a trigonal bipyramid geometry (Fig. S2b). The bond lengths of W-O, Zn-O and Zn-N range from 1.720(16) − 2.354(15) Å, 2.031(16) − 2.217(16) Å and 2.031(16) − 2.217(16) Å, respectively, which are all in accord with the range of the related compounds [30]. Based on the bond valence-sum (BVS) calculation on **LCU-22**, the oxidation states of the As, W and Zn atoms are + 3, + 6 and + 2 (Table S3), respectively, which are consistent with the XPS spectra [31].

Finally, four $[Zn(1\text{-ipIM})_3]^{2+}$ subunits connect the central $[Zn_6(AsW_9O_{33})_2(1\text{-ipIM})_6]^{6-}$ cluster with its four neighbors (Fig. 1c), thus forming a three-dimensional open framework (Fig. 2a). The $[Zn_6(AsW_9O_{33})_2(1\text{-ipIM})_6]^{6-}$ clusters in **LCU-22** are arranged in a top-and-side alternate pattern with each adjacent cluster, and this interlaced arrangement leads to the formation of two kinds of unique cavities about 4.2 and 5.5 Å, respectively (Fig. S6). If taking the $[Zn_6(AsW_9O_{33})_2(1\text{-ipIM})_6]^{6-}$ cluster as node, we find that this 3D open framework is a 4-connected ***lvt*** network with an extended Schläfli symbol of $\{4^2 0.8^4\}$. Two equivalent networks adopt 2-fold interpenetration to avoid the large voids existed in the single net (Fig. 2b). According to Blatov's classification [32], the type of interpenetration is assigned to class Ia, Zt = 2, which suggests two identical interpenetrated nets are generated by only translations with the translating vectors of [0, 0, 1].

The IR spectrum of **LCU-22** exhibits the typical ν(W-O_d), ν(W-O_b), and ν(W-O_c) stretching vibrations of the $[AsW_9O_{33}]^{9-}$ anion [33] and the C-N and C-C bonds stretching vibrations of 1-ipIM (Fig. S7). The PXRD of **LCU-22** was illustrated in Fig. S8 and the results indicated that the diffraction peaks of both simulated and experimental patterns match well in relevant positions, suggesting the good phase purity of **LCU-22**. The thermal stability of **LCU-22** was determined by thermal gravimetric analysis (TGA). TGA of **LCU-22** was performed under N_2 atmosphere from 25 °C to 750 °C. As illustrated in Fig. S9, The TG curve shows that **LCU-22** is stable below 250 °C. The weight loss process gives approximate 3.8 % (calc. 3.4 %) for **LCU-22** in the range of 60 – 295 °C, corresponding to the decomposition of the free 1-ipIM molecules. And there is a continuous weight loss in the range of 295–750 °C, possibly suggests the structural collapse of the polyoxometalate framework. On the other hand, the chemical stability of **LCU-22** was confirmed by comparing PXRD patterns. The as-synthesized samples of **LCU-22** were immersed in HCl and NaOH aqueous solutions in the pH range of 1 − 12 and various solvents (EtOH, MeOH, DCM, DMF, H_2O and THF) for 24 h at room temperature, respectively. As shown in Fig. 3a, **LCU-22** maintains the integrity of frameworks in acid and alkaline aqueous solutions with pH = 2 − 11 for at least 24 h, while pH values reached 1 and 12, respectively, there are something discrepant in the PXRD patterns with the as-synthesized **LCU-22**. In addition, the structure of **LCU-22** is well retained in strongly polar solvent DMF to weak polar solvent DCM, as revealed by PXRD patterns (Fig. 3b). Accordingly, the above results suggested that **LCU-22** exhibits excellent structure stability in wide pH range and various solvents. The reasons of good stability of **LCU-22** are as followed: (1) high-valence tungsten and zinc ions could form strong

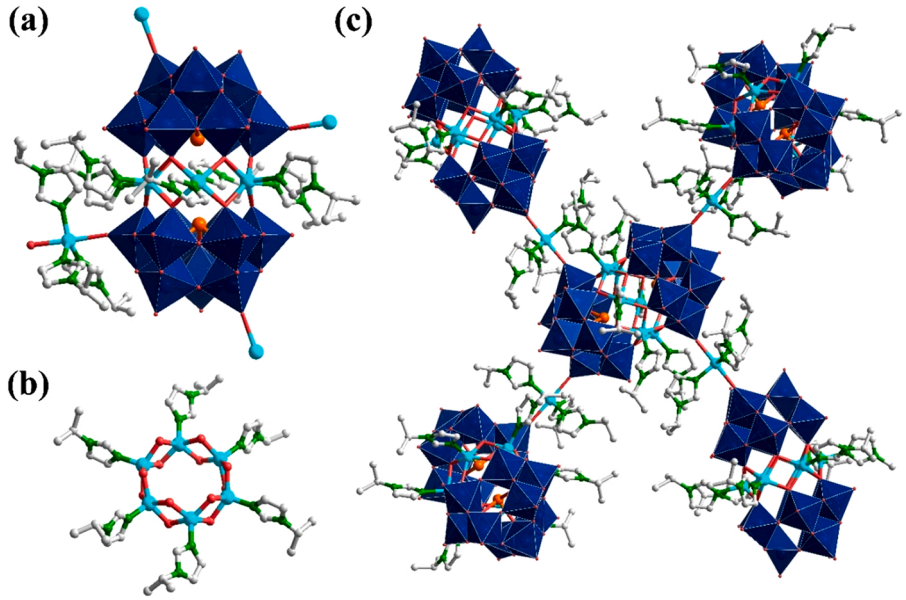

Fig. 1. (a) The cluster structure in **LCU-22**; (b) the ring-like $[Zn_6(1\text{-ipIM})_6]^{12+}$ cluster in the middle; (c) the connection of central $[Zn_6(AsW_9O_{33})_2(1\text{-ipIM})_6]^{6-}$ cluster to the neighbor four clusters. Color codes: W, deep blue; Zn, turquoise; As, orange; O, red; N, green; C, gray.

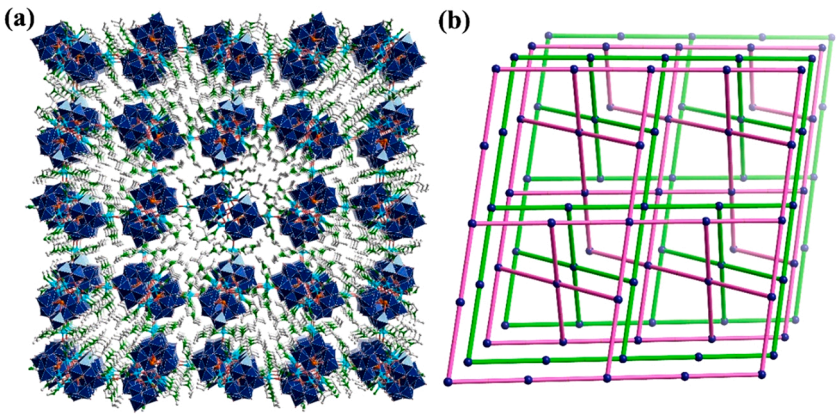

Fig. 2. (a) The 3D open framework of **LCU-22**; (b) Schematic presentations of the 2-fold interpenetrated 4-connected ***lvt*** networks.

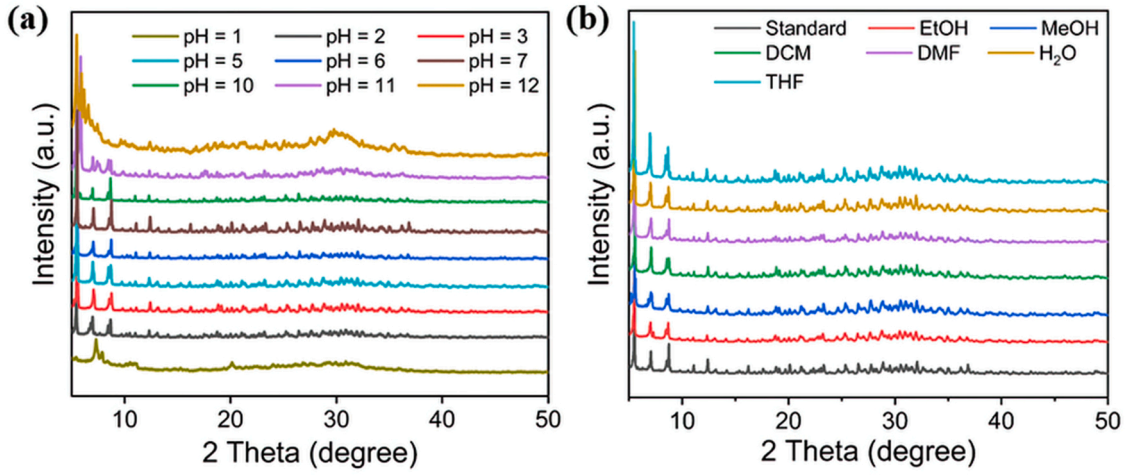

Fig. 3. PXRD patterns of **LCU-22** after immersed in (a) aqueous solutions with different pH values and (b) various solvents at room temperature for 24 h.

coordination bonds with oxygen and nitrogen atoms; (2) the saturated coordination modes of each metal atom could maintain the stability of the POM-OF. (3) The interpenetrated ***lvt*** open framework structures could further enhance the stability. These above factors endow **LCU-22** with commendable stability, which plays an important role in practical catalytic applications.

To understand the mechanism of the photocatalytic redox, the UV-Vis diffuse reflectance spectrum was measured to examine the optical response of **LCU-22 (**Fig. S10). The optical absorption of **LCU-22** is noticeably extended to the visible region. These band absorptions are assigned to the synergic interaction between sandwich-type polyoxotungstates and Zn^{II}. The visible-light harvesting capability induces the more photogenerated charge carriers in **LCU-22** under visible-light illumination, which consequently results in the improved photocatalytic performance [34].

In order to investigate the photocatalytic performance of **LCU-22**, the photoelectrochemical characterization as typical semiconductor-type photocatalysts has been carried out. The diffuse reflectance using the Kubelka-Munk (K-M) function (Fig. 4a) shows that the band-gap energy (E_g) of **LCU-22** is 2.95 eV. The Mott-Schottky plots were further measured at frequencies of 2000, 2500, 3000 Hz, respectively, using a standard three-electrode system, including Pt wire as the counter electrode, Ag/AgCl as reference electrode and the prepared photocatalyst (2 mg, dispersed in 50 μL of Nafion and 950 μL of ethanol mixed solution) as the working electrode, and using 0.2 M Na_2SO_4 aqueous solution as the electrolyte (Fig. 4b). The positive slope of the obtained C^{2-} values was consistent with those reported for n-type semiconductors. As a result, the lowest unoccupied molecular orbital (LUMO) level of **LCU-22** was − 1.24 V vs. Ag/AgCl (−1.04 V vs. NHE), and the corresponding highest occupied molecular orbital (HOMO) level was calculated to be 1.91 V vs. NHE ($E_{HOMO} = E_g - E_{LUMO}$).

As shown in Fig. 4c, the photocurrent response measurement of **LCU-22** revealed a fast and periodic on/off responses on eight consecutive rounds with intermittent irradiation, indicating the low recombination efficiency of photogenerated electron-hole pairs and enhanced charge carrier's separation, facilitating the electron transfer during the photocatalysis process. Moreover, electrochemical impedance spectra (EIS) (Fig. 4d) and linear sweep voltammetry (LSV) of **LCU-22** have also been tested (Fig. S13). These results strongly indicates that **LCU-22** has great potential to be a photocatalyst.

XPS is one of the most important analytical techniques for investigating the chemical valence of POMs materials. To gain further insights into the element valence in **LCU-22**, XPS of the As 3d, Zn 2p and W 4f were performed. As shown in Fig. S14, three characteristic peaks of As, Zn and W in POMs were observed, respectively. The core level of As 3d shows a weak peak at the binding energy of 44.28 eV in **LCU-22**. The binding energies of the 3d core levels of As are in good agreement with the values in the literature for As^{III} [35]. The peak observed at 1021.57 eV in the XPS of **LCU-22** can be assigned to the $2p_{3/2}$ and $2p_{1/2}$ core levels of the Zn^{II} species [36]. Two peaks located at 35.4 and 37.5 eV in the XPS of **LCU-22** correspond to the core levels of W $4f_{5/2}$ and W $4f_{7/2}$ in the W^{VI} ions [37]. Furthermore, the appearance of higher binding energy shake-up satellite peaks located at approximately 40.3 eV corresponds to energy loss features for WO_3 [38].

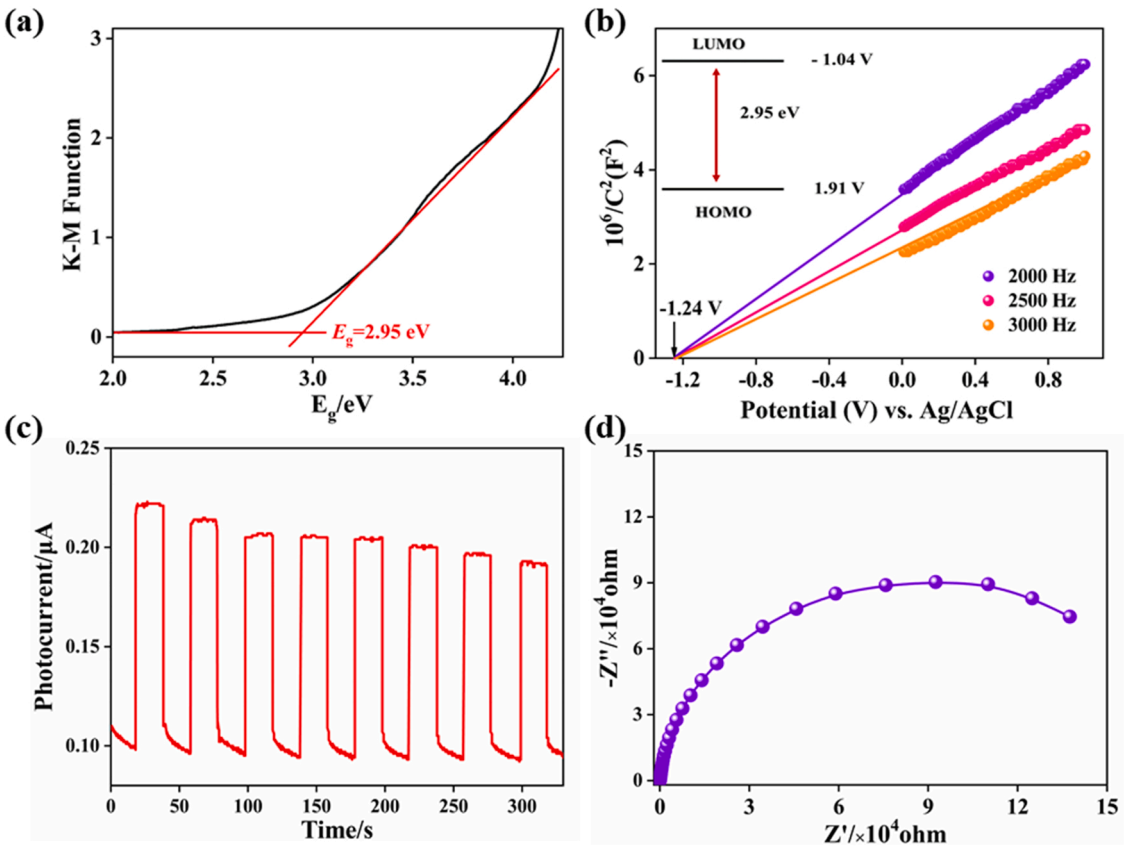

Fig. 4. (a) Band-gap energy of **LCU-22** converted from the diffuse reflectance using the K-M function; (b) Mott-Schottky plots for **LCU-22** in 0.2 M Na_2SO_4 aqueous solution at different frequencies, using Ag/AgCl as the reference electrode; (c) photocurrent responses of **LCU-22** under the transient period Xe-lamp irradiation; (d) electrochemical impedance spectra of **LCU-22**.

*3.2. Catalytic activities of **LCU-22** in photosynthesis of pyridine derivatives*

Pyridine derivatives, such as nifedipine, vitamin B_3 and vitamin B_6, are the most main classes of potentially bioactive structures found in natural products and widely used in pharmaceutical industry and many excellent results have been reported [39]. However, their syntheses are still highly challenging regarding to the stoichiometric/costly oxidant, harsh reaction conditions, two-step reaction and noble metal catalysts [40–42]. Thus, the development of new organic catalysis systems for the pyridine derivatives under environmentally friendly conditions is still in great demand. It is well known that Zn-containing complexes have exhibited excellent Lewis acid catalytic activities in photocatalytic reactions [43]. Besides, polyoxotungstates with multiple redox-active sites also presented versatile catalytic activity and sustained their structural integrity well during photooxdiation of primary amine coupling [44]. Therefore, the combination of Zn-containing complexes and polyoxotungstates with bifunctional photocatalytic properties is highly desirable. In this work, photo-driven organic reactions catalyzed by **LCU-22** provided a promising route for one-step synthesis of pyridine derivatives.

Preliminarily, we performed the three-component reaction of benzaldehyde, methyl acetoacetate and ammonium acetate at room temperature to evaluate the photocatalytic activities of **LCU-22**. Initially, different light sources, including UV, blue, green, red and white LED light were successively screened (Fig. 5a). Surprisingly, the reaction irradiated by white LED light in the presence of **LCU-22** displayed good efficiency (87 % yield). Next, the reaction was conducted in the absence of catalyst and afforded the trace desired products, which proved that the catalyst is critical to this three-component reaction (Table S5, entry 1). The screening of the different catalysts revealed that eco-friendly and renewable catalyst **LCU-22** played a unique role in this transformation at 1 atm O_2 atmosphere under a 10 W white LED irradiation, which may be caused by the synergetic effect of Zn species and sandwich ATs (Fig. 5b). Further optimization revealed that MeOH was superior to other solvents, such as DMF, DMSO, H_2O and MeCN (Fig. 5c). When the loading of **LCU-22** was increased to 10 mg, a favorable yield of pyridine derivatives was obtained (Fig. 5d). On the other hand, only a 17 % yield of **1a** was detected for 48 h in the dark condition, which indicated that catalytic activity of **LCU-22** was mainly induced by visible light (Table S5, entry 9). Moreover, to evaluate the influence of each active center in the photosynthesis of pyridine derivatives, the following control experiments were designed and carried out (Table S5). When the mixture of compound $ZnCl_2$ and 1-ipIM ligand with mole ratio of 1:6 was used as catalyst, the yield of pyridine derivative **1a** was 22 % (Table S5, entry 3). Meanwhile, using POMs (Na_8[A-$HAsW_9O_{34}$]·11 H_2O) as catalyst, the reaction could also be finished (the yield of pyridine derivatives is 53 %, Table S5, entry 4) which is obviously lower than using **LCU-22** as catalyst. Above results means that Zn and POMs active centers in **LCU-22** play the Lewis acid and oxidation sites role in the photocatalytic reaction, respectively, but their combination, namely **LCU-22**, can significantly enhance the catalytic activity over each single component.

With the above optimized reaction conditions, the photosynthesis of pyridines using **LCU-22** was successfully extended to various substrates under visible light irradiation and the corresponding results are listed in Table 1. First, diverse substitutions, such as -MeO, -Me, -Cl, -Br and -NO_2 at the *para*-position of benzaldehyde were successfully screened to afford the targeted products in admirable yields, suggesting the electron-withdrawing or electron-donor groups did not affect the catalytic efficiency (Table 1, entries 2–6, except entry 4). Especially, the methyl group at the *meta*-position of benzaldehyde could also achieve the ideal yield under the same conditions (Table 1, entry 4). Significantly, 5-

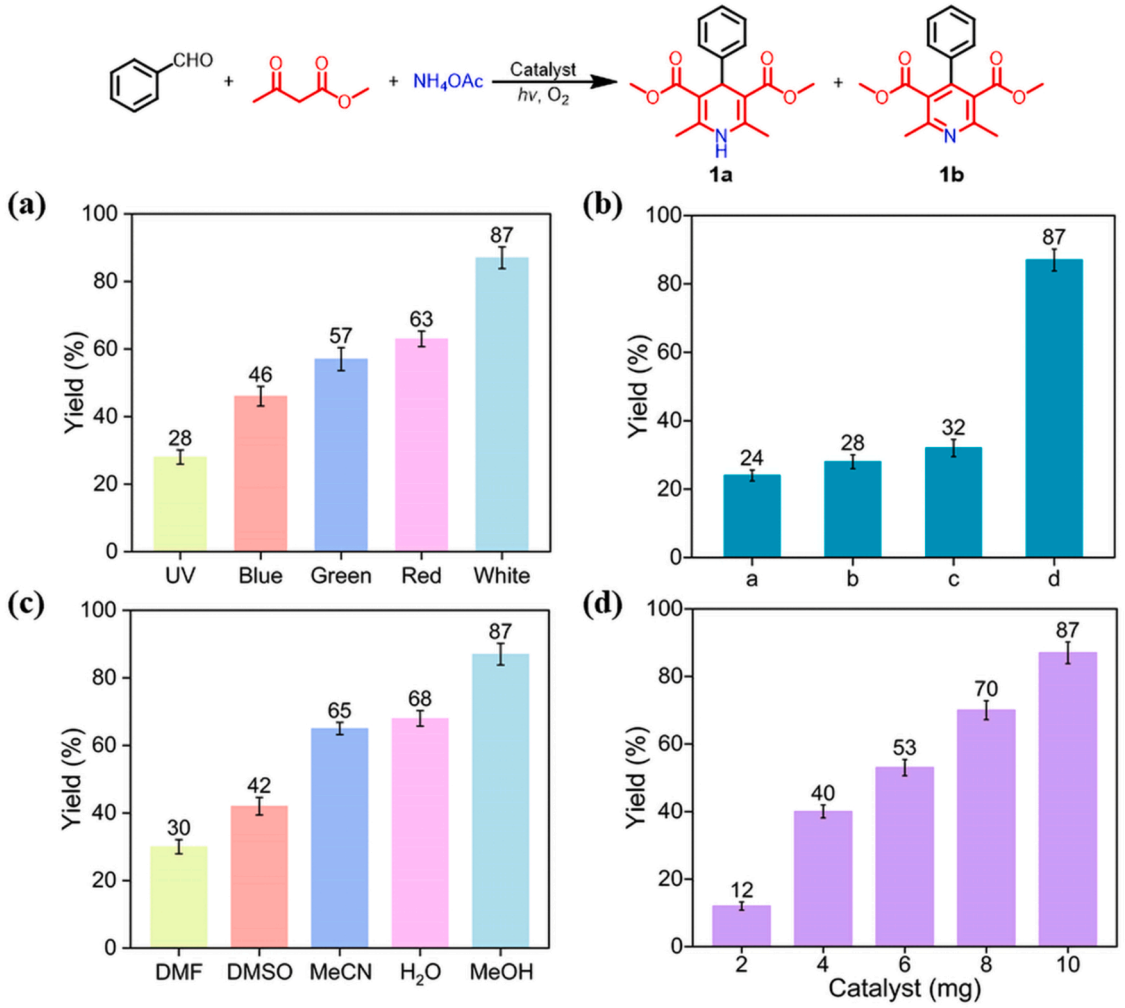

Fig. 5. Optimization of the reaction conditions for the photosyntheses of pyridine derivatives. Reaction conditions: benzaldehyde (1 mmol), methyl acetoacetate (2 mmol), ammonium acetate (1 mmol), catalyst (10 mg) and 2 mL solvent under 1 atm O_2, white LED light (10 W), room temperature, 48 h. (a) The effect of different photosources; (b) the effect of different catalysts, a) $ZnCl_2$; b) Na_2WO_4; c) the mixture of $ZnCl_2$ and Na_2WO_4; d) **LCU-22**; (c) the effect of different solvents; (d) the effect of different amounts of **LCU-22**. The yields in the figure were referred to the sum yields of the two pyridine derivatives (**1a** and **1b**).

hydroxymethylfurfural (HMF), the promising building blocks for bio-based chemicals [45], is also active in the reaction under operational conditions to deliver the yields of 60 % (Table 1, entry 8). In addition, 2-thiophenecarboxaldehyde and 2-pyridinecarboxaldehyde as substrates can also obtained the desired products in the favorable yields (Table 1, entries 9–10). However, for the *ortho*-substituted aromatic aldehydes, no desired product was detected which might be caused by the steric hindrance of *ortho*-substituted aromatic aldehydes in the reaction (Table 1, entry 11).

The reusability and heterogeneity of **LCU-22** was tested using the photocatalytic reaction of benzaldehyde, methyl acetoacetate and ammonium acetate as the model. After completion of the three photocatalytic cycles, the catalyst can be easily separated from the reaction mixture by centrifugation. Most importantly, there was no significant decrease in yields after three cycles (Fig. S15; 1st run, yield 87 %; 2nd run, yield 86 %; 3rd run, yield 84 %), indicating excellent cycling stability of the **LCU-22**. The results achieved even match some noble-metal-based catalyst reported in the literature [46]. In the leaching test for the photosynthesis of pyridine derivates, (Fig. S16), **LCU-22** was removed from the reaction system after 24 h, and the yield of pyridines in the filtrate hardly reacted for the next 24 h. Besides, the IR spectra and PXRD patterns of the recovered catalyst were consistent with the fresh catalyst (Fig. 6a, b), and no significant change can be observed in the XPS spectra of the W and Zn ions in **LCU-22** after reusing three times (Fig. 6c, d).

In order to monitor whether there might be possible changes in the morphologies of the microcrystallites before and after photocatalysis reaction of **LCU-22**, the scanning electron microscope (SEM) images of **LCU-22** after the reaction displayed block-like shape with an average length size of 20 μm, which matched well with those of before the reaction (Fig. S17). An examination of the SEM images of the POMs reveals its excellent structural stability and the microcrystalline structure can be clearly observed at low magnification. An SEM-EDS mapping of **LCU-22** further indicates that the structure is stable after the catalytic reaction. These results suggested that the catalyst **LCU-22** remains basically identical shape before and after the photocatalytic reaction.

In order to investigate the reaction mechanism, a series of control experiments were carried out. In the absence of **LCU-22**, O_2, or light, trace amounts of desired products were detected, indicating the essential roles of the above factors in the formation of pyridines. In addition, to further study the reaction process, the reaction intermediates **9–12** were successively monitored by GC-MS, respectively (Figs. S20-S22). When the radical scavenger 2,2,6,6-tetramethylpiperidin-1-oxyradical (TEMPO, 4.0 mmol) was added to probe the radical nature of the reactions, no corresponding products **1a** and **1b** were detected, suggesting that the radical was involved in the reaction. Furthermore, the role of O_2 was confirmed by electron spin resonance (ESR) experiments in the photocatalytic synthesis of pyridine derivatives using 5,5-dimethyl-1-

Table 1
The results of synthesis of pyridines catalyzed by **LCU-22**[a].

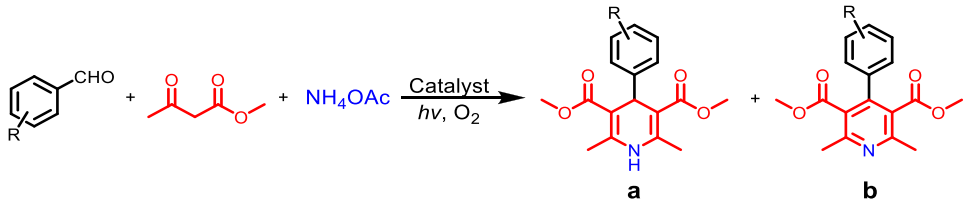

Entry	Substrates	Products of **a**	Products of **b**	Yields (%)[b]
1		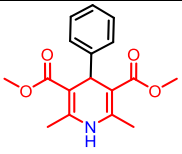 **1a**	 **1b**	87 (62:25)
2	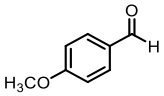	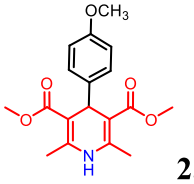 **2a**	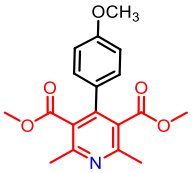 **2b**	81 (59:22)
3	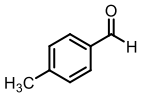	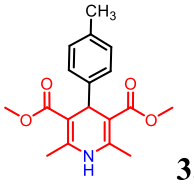 **3a**	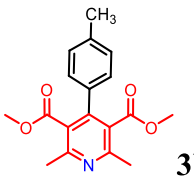 **3b**	80 (57:23)
4	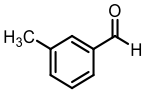	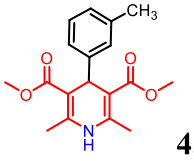 **4a**	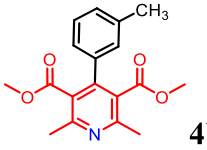 **4b**	76(54: 22)
5	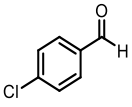	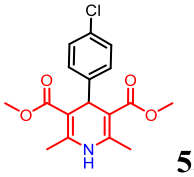 **5a**	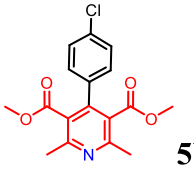 **5b**	61 (38:23)

(*continued on next page*)

Table 1 (*continued*)

6	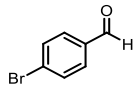	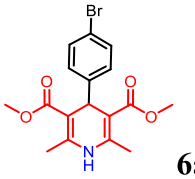 **6a**	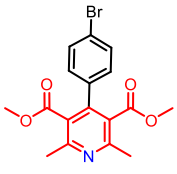 **6b**	53 (35:18)
7	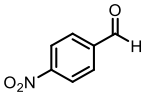	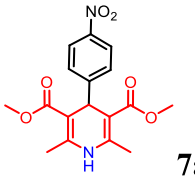 **7a**	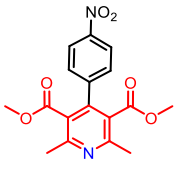 **7b**	62 (42:20)
8	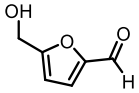	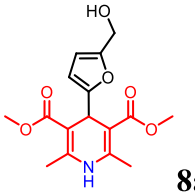 **8a**	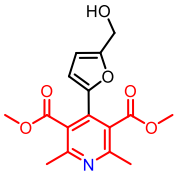 **8b**	60 (49:11)
9	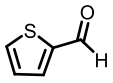	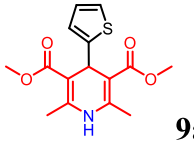 **9a**	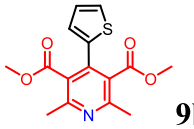 **9b**	62 (50:12)
10	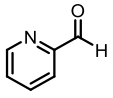	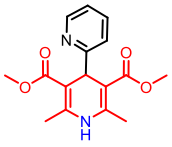 **10a**	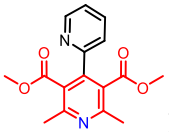 **10b**	65 (48:17)
11	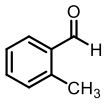	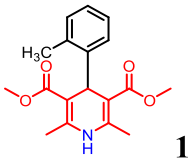 **11a**	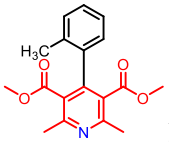 **11b**	trace

[a]Reaction conditions: aromatic aldehydes (1 mmol), methyl acetoacetate (2 mmol), ammonium acetate (1 mmol), **LCU-22** (0.15 mol%) and MeOH (2 mL) under 1 atm O_2, white LED light (10 W), 48 h. [b]Isolated yields, ratios in brackets are the ratios of the yield of products **a** and **b**.

pyrroline-N-oxide (DMPO) as superoxide radical trapping agent, the superoxide radical $O_2^{\bullet-}$ could be detected under the given conditions, while no ESR signals were monitored in the dark. The above results corroborated that $O_2^{\bullet-}$ could be generated in the presence of **LCU-22** under light conditions (Fig. S25) [47].

On the basis of the controlled experiments and previous results [48, 49], a proposed reaction mechanism for cascade Hantzsch and dehydrogenation over the **LCU-22** is illustrated in Scheme 1. Frist, the intermediate **9** was generated by condensation of benzaldehyde and methyl acetoacetate catalyzed by **LCU-22**. After that, intermediate **10** was produced when the ammonium acetate was reacted with methyl acetoacetate, followed by the cyclization and condensation reactions with **9** and gave the corresponding dihydropyridine **1a**. In the next stages, upon visible light irradiation, the excited species **LCU-22*** is formed and then it reacted with dihydropyridine **1a** to give a radical cation and radical anion **LCU-22**$^{\bullet-}$. Next, the radical anion **LCU-22**$^{\bullet-}$ actives the molecule oxygen, producing the $O_2^{\bullet-}$ and regenerating **LCU-22** [50]. The radical cation and $O_2^{\bullet-}$ underwent the proton abstraction and

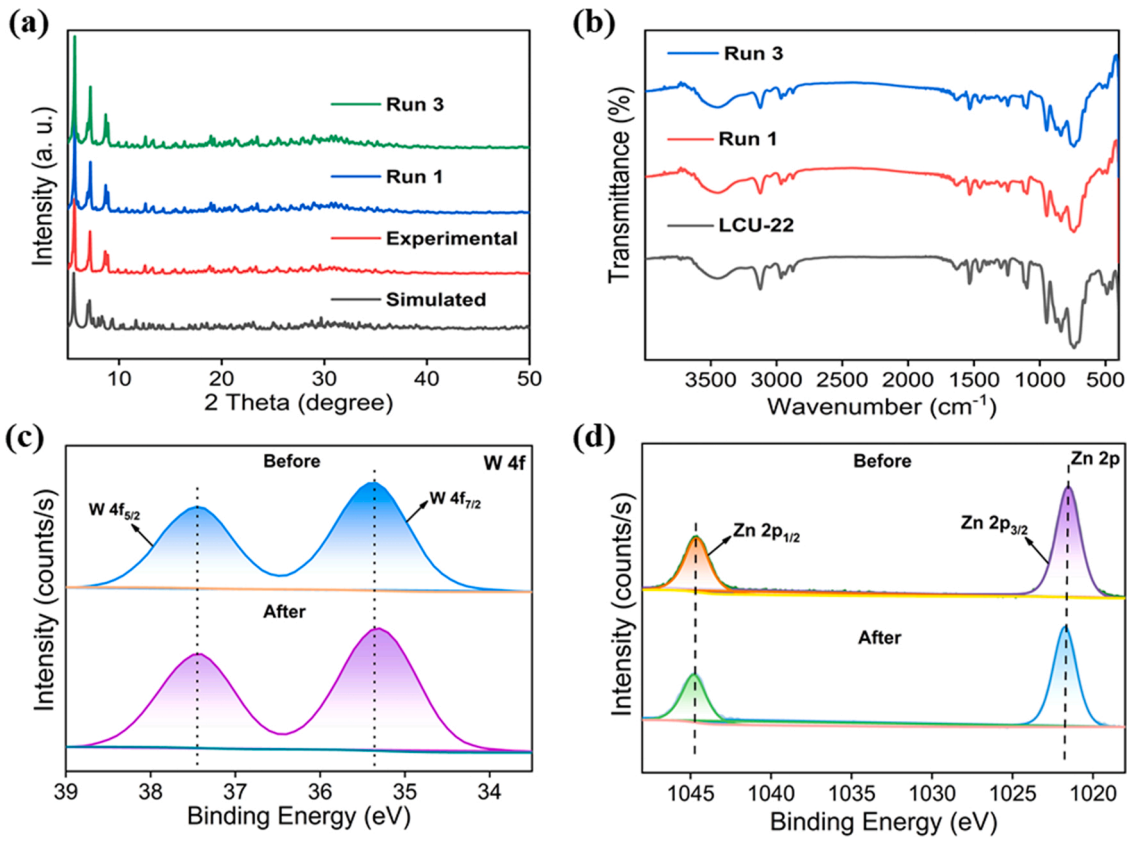

Fig. 6. (a) The PXRD of **LCU-22** before and after three runs reactions; (b) the IR of **LCU-22** before and after three runs reaction; (c) the XPS of W 4f in **LCU-22** before and after three runs reactions; (d) the XPS of Zn 2p in **LCU-22** before and after three runs reactions.

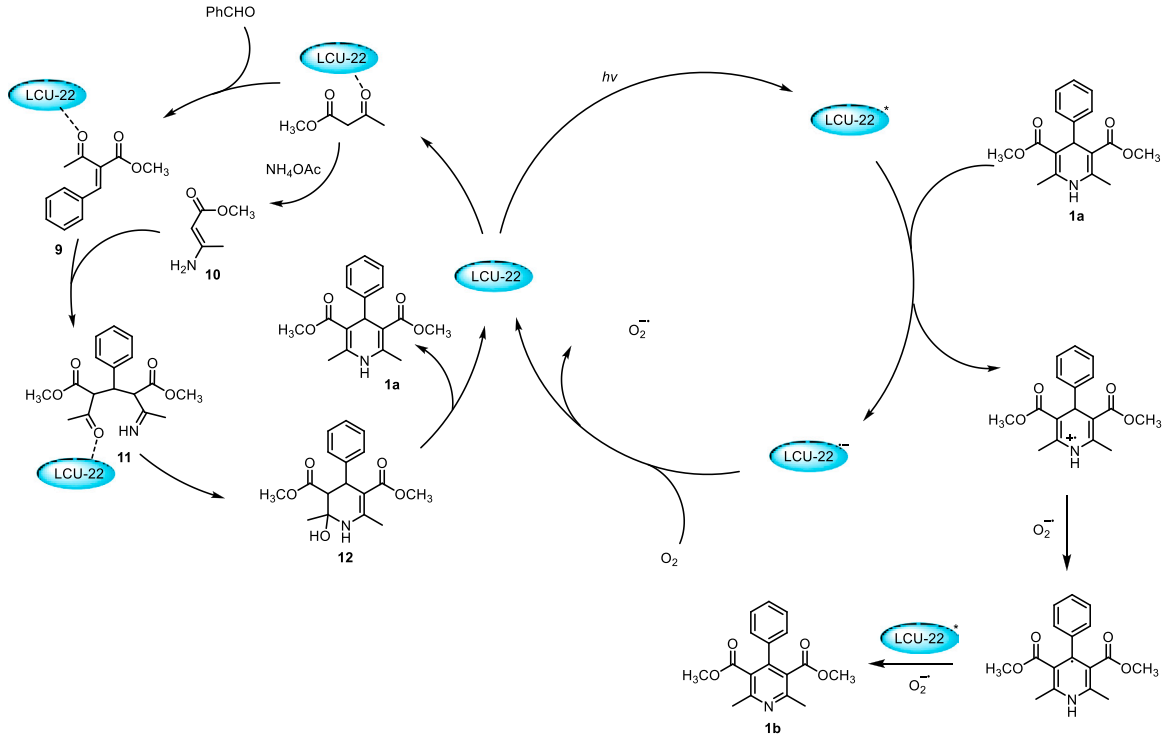

Scheme 1. Proposed pathways for cascade Hantzsch and dehydrogenation over **LCU-22.**

finally afforded the desired pyridine product **1b** [51].

4. Conclusions

In summary, a straightforward and gram-scale synthesis method was developed to produce an unprecedented 2-fold interpenetrated ***lvt*** polyoxometalate-based open framework **LCU-22**. Specifically, POM-OF node in **LCU-22** is a Zn_6 ring seamed trivacant ($[Zn_6(AsW_9O_{33})_2]$) cluster, which is quadruply linked by $[Zn(1\text{-ipIM})_3]^{2+}$ units to form the final robust 3D framework, exhibiting highly stable in various solvents and wide pH range. Remarkably, this is the first report on the sandwich-type POMs photocatalyzed one-step synthesis of pyridine derivatives using molecule oxygen as green oxidant. **LCU-22** exhibited extraordinary heterogeneous catalytic activities due to synergistic effect between the Zn-complexes and sandwich-type POMs (yields up to 87 %). Mechanistically, it is speculated that the Lewis acid Zn site on the **LCU-22** and the oxidation site POMs units act in a synergistic manner to lower the energy barrier required for the reaction, allowing the reaction to proceed quickly. Moreover, **LCU-22** as robust catalyst could be regenerated and reused at least three times in subsequent reactions without significant loss of activities. Further research on the development of the novel photo-responsive POMs materials for other potential catalytic reactions is in progress.

CRediT authorship contribution statement

X. Huang and **D. Sun** proposed the research project and guided the whole experiments. **S. Liu, G. Liu, Y. Tao, C. Wang, Z. Li, H.** Wang conducted the syntheses and characterization of complexes, and drafted the manuscript. **Y. Zhang, Z. Zhou, G. Shen**, and **Z. Xue** performed catalysis experiments and related characterizations.

Declaration of Competing Interest

The authors declare the following financial interests/personal relationships which may be considered as potential competing interests: Di Sun reports financial support was provided by National Natural Science Foundation of China.

Data availability

Data will be made available on request.

Acknowledgement

This work was financially supported by National Natural Science Foundation of China (No. 21871125, 22171139, 21801145, 21901122, and 22171164), the Natural Science Foundation of Shandong Province, China (No. ZR2019MB043 and ZR2019QB022), Shandong Provincial Key R&D Program/Major Science and Technology Innovation Project of Shandong Province (2019JZZY020230) and the Construction Project of Quality Curriculum for Postgraduate Education of Shandong Province (No. SDYKC19057).

Associated content

Electronic Supplementary Information (ESI) available: [details of any supplementary information available should be included here]. See DOI: 10.1039/x0xx00000x. Crystal data of **LCU-22**, Selected Bond lengths [Å] and angles [°] for **LCU-22**, The IR spectrum and PXRD patterns of **LCU-22**, Scanning electron microscopy image of **LCU-22**, Morphology images and elemental mappings of **LCU-22**, The ^{1}H NMR and ^{13}C NMR of products.

Appendix A. Supporting information

Supplementary data associated with this article can be found in the online version at doi:10.1016/j.apcatb.2022.122134.

References

[1] T. Wang, T. Ji, W. Chen, X. Li, W. Guan, Y. Geng, X. Wang, Y. Li, Z. Kang, Polyoxometalate film simultaneously converts multiple low-value all-weather environmental energy to electricity, Nano Energy 68 (2020), 104349, https://doi.org/10.1016/j.nanoen.2019.104349.
[2] S. Zheng, H. Xue, H. Pang, Supercapacitors based on metal coordination materials, Coord. Chem. Rev. 373 (2018) 2–21, https://doi.org/10.1016/j.ccr.2017.07.002.
[3] J. Guo, D. Ma, F. Sun, G. Zhuang, Q. Wang, A.M. Al-Enizi, A. Nafady, S. Ma, Substituent engineering in g-C_3N_4/COF heterojunctions for rapid charge separation and high photo-redox activity, Sci. China Chem. 65 (2022) 1704–1709, https://doi.org/10.1007/s11426-022-1350-1.
[4] A.S. Belousov, E.V. Suleimanov, Application of metal–organic frameworks as an alternative to metal oxide-based photocatalysts for the production of industrially important organic chemicals, Green Chem. 23 (2021) 6172–6204, https://doi.org/10.1039/D1GC01690C.
[5] X. Dong, F. Zhang, F. Huang, X. Lang, Pyrene-based conjugated microporous polymers for red light-powered oxidation of amines to imines, Appl. Catal. B Environ. 318 (2022), 121875, https://doi.org/10.1016/j.apcatb.2022.121875.
[6] W. Shang, Y. Li, H. Huang, F. Lai, M.B. Roeffaers, B. Weng, Synergistic redox reaction for value-added organic transformation via dual-functional photocatalytic systems, ACS Catal. 11 (2021) 4613–4632, https://doi.org/10.1021/acscatal.0c04815.
[7] S. Chu, B. Zhang, X. Zhao, H.S. Soo, F. Wang, R. Xiao, H. Zhang, Photocatalytic conversion of plastic waste: from photodegradation to photosynthesis, Adv. Energy Mater. 12 (2022), 2200435, https://doi.org/10.1002/aenm.202200435.
[8] W. Sheng, X. Wang, Y. Wang, S. Chen, X. Lang, Integrating TEMPO into a metal-organic framework for cooperative photocatalysis: selective aerobic oxidation of sulfides, ACS Catal. 12 (2022) 11078–11088, https://doi.org/10.1021/acscatal.2c02519.
[9] F. Raziq, A. Hayat, M. Humayun, S.K. Mane, M.B. Faheem, A. Ali, Y. Zhao, S. Han, C. Cai, W. Li, D. Qi, J. Yi, X. Yu, M.B. Breese, F. Hassan, F. Ali, A. Mavlonov, K. Dhanabalan, L. Qiao, Photocatalytic solar fuel production and environmental remediation through experimental and DFT based research on CdSe-QDs-Coupled P-doped-g-C_3N_4 composites, Appl. Catal. B Environ. 270 (2020), 118867, https://doi.org/10.1016/j.apcatb.2020.118867.
[10] K. Guo, X. Zhu, L. Peng, Y. Fu, R. Ma, X. Lu, F. Zhang, W. Zhu, M. Fan, Boosting photocatalytic CO_2 reduction over a covalent organic framework decorated with ruthenium nanoparticles, Chem. Eng. J. 405 (2021), 127011, https://doi.org/10.1016/j.cej.2020.127011.
[11] K.G. Forson, B.O. Bohman, C.Z. Wayment, R.N. Owens, C.E. McKnight, R.C. Davis, L.R. Stillwell, S.J. Smith, D.J. Michaelis, Retraction of "medium and large N-heterocycle formation via allene hydroamination with a bimetallic Rh(II) catalyst", J. Am. Chem. Soc. 144 (2022) 5668–5669, https://doi.org/10.1021/jacs.2c02451.
[12] R.C. DiPucchio, S.-C. Rosca, L.L. Schafer, Hydroaminoalkylation for the catalytic addition of amines to alkenes or alkynes: diverse mechanisms enable diverse substrate scope, J. Am. Chem. Soc. 144 (2022) 11459–11481, https://doi.org/10.1021/jacs.1c10397.
[13] Y. Zhang, T. Song, X. Zhou, Y. Yang, Oxygen-vacancy-boosted visible light driven photocatalytic oxidative dehydrogenation of saturated N-heterocycles over Nb_2O_5 nanorods, Appl. Catal. B Environ. 316 (2022), 121622, https://doi.org/10.1016/j.apcatb.2022.121622.
[14] T. Miyakoshi, N.E. Niggli, O. Baudoin, Remote construction of N-heterocycles via 1,4-palladium shift-mediated double C−H activation, Angew. Chem. . Ed. 61 (2022), e202116101, https://doi.org/10.1002/anie.202116101.
[15] S. Liu, X. Cheng, Insertion of ammonia into alkenes to build aromatic N-heterocycles, Nat. Commun. 13 (2022) 425, https://doi.org/10.1038/s41467-022-28099-w.
[16] A. Papastathopoulos, N. Lougiakis, I.K. Kostakis, P. Marakos, N. Pouli, H. Pratsinis, D. Kletsas, New bioactive 5-arylcarboximidamidopyrazolo[3,4-c]pyridines: synthesis, cytotoxic activity, mechanistic investigation and structure-activity relationships, Eur. J. Med. Chem. 218 (2021), 113387, https://doi.org/10.1038/s41467-022-28099-w.
[17] Y. Ren, W. Dai, S. Guo, L. Dong, S. Huang, J. Shi, B. Tong, N. Hao, L. Li, Z. Cai, Y. Dong, Clusterization-triggered color-tunable room-temperature phosphorescence from 1,4-dihydropyridine-based polymers, J. Am. Chem. Soc. 144 (2022) 1361–1369, https://doi.org/10.1021/jacs.1c11607.
[18] H.-C. Yu, S.M. Islam, N.P. Mankad, Cooperative heterobimetallic substrate activation enhances catalytic activity and amplifies regioselectivity in 1,4-hydroboration of pyridines, ACS Catal. 10 (2020) 3670–3675, https://doi.org/10.1021/acscatal.0c00515.
[19] S. Karamzadeh, E. Sanchooli, A.R. Oveisi, S. Daliran, R. Luque, Visible-LED-light-driven photocatalytic synthesis of n–heterocycles mediated by a polyoxometalate–containing mesoporous zirconium metal-organic framework, Appl. Catal. B Environ. 303 (2022), 120815, https://doi.org/10.1016/j.apcatb.2021.120815.
[20] Q. Liu, Q. Zhang, W. Shi, H. Hu, J. Zhuang, X. Wang, Self–assembly of polyoxometalate clusters into two–dimensional clusterphene structures featuring

hexagonal pores, Nat. Chem. 14 (2022) 433–440, https://doi.org/10.1038/s41557-022-00889-1.
[21] Z. Li, J. Zhang, X. Jing, J. Dong, H. Liu, H. Lv, Y. Chi, C. Hu, A polyoxometalate@covalent triazine framework as a robust electrocatalyst for selective benzyl alcohol oxidation coupled with hydrogen production, J. Mater. Chem. A 9 (2021) 6152–6159, https://doi.org/10.1039/D0TA09421H.
[22] L. Chen, W. Chen, X. Wang, Y. Li, Z. Su, E. Wang, Polyoxometalates in dye–sensitized solar cells, Chem. Soc. Rev. 48 (2019) 260–284, https://doi.org/10.1039/C8CS00559A.
[23] G. Paille, M. Gomez-Mingot, C. Roch-Marchal, B. Lassalle-Kaiser, P. Mialane, M. Fontecave, C. Mellot-Draznieks, A. Dolbecq, A fully noble metal-free photosystem based on cobalt-polyoxometalates immobilized in a porphyrinic metal-organic framework for water oxidation, J. Am. Chem. Soc. 140 (2018) 3613–3618, https://doi.org/10.1021/jacs.7b11788.
[24] S. Zheng, M. Wang, G. Yang, Extended architectures constructed from sandwich tetra–metal–substituted polyoxotungstates and transition-metal complexes, Chem. Asian J. 2 (2007) 1380–1387, https://doi.org/10.1002/asia.200700166.
[25] T. Yamase, K. Fukaya, H. Nojiri, Y. Ohshima, Ferromagnetic exchange interactions for Cu_6^{12+} and Mn_6^{12+} hexagons sandwiched by two B-α-$[XW_9O_{33}]^{9-}$ (X = As^{III} and Sb^{III}) ligands in D_{3d}-symmetric polyoxotungstates, Inorg. Chem. 45 (2006) 7698–7704, https://doi.org/10.1021/ic060666f.
[26] T. Yamase, H. Ishikawa, A. Hiroko, K. Fukaya, H. Nojiri, H. Takeuchi, Molecular magnetism of M_6 hexagon ring in D_{3d} symmetric $[(MCl)_6(XW_9O_{33})_2]^{12-}$ (M = Cu^{II} and Mn^{II}, X = Sb^{III} and As^{III}), Inorg. Chem. 51 (2012) 4606–4619, https://doi.org/10.1021/ic202513q.
[27] S. Chang, Y. Qi, E. Wang, Z. Zhang, Two novel sandwiched-type polyoxotungstates containing Zn_6 transition-metal cluster: syntheses, structures and luminescent property, Inorg. Chim. Acta 362 (2009) 453–457, https://doi.org/10.1016/j.ica.2008.04.048.
[28] G.M. Sheldrick, A short history of SHELX, Acta Cryst. A64 (2008) 112–122, https://doi.org/10.1107/S0108767307043930.
[29] X. Huang, X. Gu, Y. Qi, Y. Zhang, G. Shen, B. Yang, W. Duan, S. Gong, Z. Xue, Y. Chen, Decavanadate-based transition metal hybrids as bifunctional catalysts for sulfide oxidation and C-C bond construction, Chin. J. Chem. 39 (2021) 2495–2503, https://doi.org/10.1002/cjoc.202100145.
[30] Y. Zhang, Z. Zhang, L. Ritter, H. Fang, Q. Wang, B. Space, Y. Zhang, D. Xue, J. Bai, New reticular chemistry of the rod secondary building unit: synthesis, structure, and natural gas storage of a series of three-way rod amide-functionalized metal-organic frameworks, J. Am. Chem. Soc. 143 (2021) 12202–12211, https://doi.org/10.1021/jacs.1c04946.
[31] H. Li, W. Chen, Y. Zhao, Y. Zou, X. Zhao, J. Song, P. Ma, J. Niu, J. Wang, Regulating the Catalytic activity of multi-rubridged polyoxometalates based on differential active site environments with six-coordinate geometry and five-coordinate geometry transitions, Nanoscale 13 (2021) 8077–8086, https://doi.org/10.1039/D1NR01447A.
[32] V.A. Blatov, L. Carlucci, G. Ciani, D.M. Proserpio, Interpenetrating metal-organic and inorganic 3d networks: a computer-aided systematic investigation. Part I. Analysis of the Cambridge Structural Database, CrystEngComm 6 (2004) 377–395, https://doi.org/10.1039/B409722J.
[33] X. Ma, K. Yu, J. Yuan, L. Cui, J. Lv, W. Dai, B. Zhou, Multinuclear transition metal sandwich-type polytungstate derivatives for enhanced electrochemical energy storage and bifunctional electrocatalysis performances, Inorg. Chem. 59 (2020) 5149–5160, https://doi.org/10.1021/acs.inorgchem.0c00382.
[34] X. Lan, Q. Li, Y. Zhang, Q. Li, L. Ricardez-Sandoval, G. Bai, Engineering donor-acceptor conjugated organic polymers with boron nitride to enhance photocatalytic performance towards visible-light-driven metal-free selective oxidation of sulfides, Appl. Catal. B Environ. 277 (2020), 119274, https://doi.org/10.1016/j.apcatb.2020.119274.
[35] H. Li, M. Yang, Z. Yuan, Y. Sun, P. Ma, J. Niu, J. Wang, Construction of one Ru_2W_{12}–cluster and six lacunary keggin tungstoarsenate leading to the larger Ru–containing polyoxometalate photocatalyst, Chin. Chem. Lett. 33 (2022) 4664–4668, https://doi.org/10.1016/j.cclet.2021.12.081.
[36] D. Li, L. Cao, T. Deng, S. Liu, C. Wang, Design of a solid electrolyte interphase for aqueous Zn batteries, Angew. Chem. Int. Ed. 60 (2021) 13035–13041, https://doi.org/10.1002/anie.202103390.
[37] Q. Chang, X. Meng, W. Ruan, Y. Feng, R. Li, J. Zhu, Y. Ding, H. Lv, W. Wang, G. Chen, X. Fang, Metal-organic cages with $\{SiW_9Ni_4\}$ polyoxotungstate nodes, Angew. Chem. Int. Ed. 61 (2022), e202117637, https://doi.org/10.1002/anie.202117637.
[38] W. Chen, H. Li, J. Song, Y. Zhao, P. Ma, J. Niu, J. Wang, Binuclear Ru(III)-containing polyoxometalate with efficient photocatalytic activity for oxidative coupling of amines to imines, Inorg. Chem. 61 (2022) 2076–2085, https://doi.org/10.1021/acs.inorgchem.1c03282.
[39] D. Xie, Y. Wang, X. Zhang, Z. Fu, D. Niu, Alkyl/Glycosyl sulfoxides as radical precursors and their use in the synthesis of pyridine derivatives, Angew. Chem. Int. Ed. 61 (2022), e202204922, https://doi.org/10.1002/anie.202204922.
[40] N. Nakamichi, Y. Kawashita, M. Hayashi, Oxidative aromatization of 1,3,5-trisubstituted pyrazolines and hantzsch 1,4-dihydropyridines by Pd/C in acetic acid, Org. Lett. 4 (2002) 3955–3957, https://doi.org/10.1021/ol0268135.
[41] D. Maiti, R. Das, T. Prabakara, S. Sen, Blue LED induced solvent-free multicomponent reactions among Aryl diazoacetates, pyridine derivatives and maleimides: direct eco-friendly synthesis of densely functionalized itaconimides, Green Chem. 24 (2022) 3001–3008, https://doi.org/10.1039/D1GC03546K.
[42] M. Pang, L. Shi, Y. Xie, T. Geng, L. Liu, R. Liao, C. Tung, W. Wang, Cobalt-catalyzed selective dearomatization of pyridines to N–H 1,4-dihydropyridines, ACS Catal. 12 (2022) 5013–5021, https://doi.org/10.1021/acscatal.2c00271.
[43] H. Han, X. Zheng, C. Qiao, Z. Xia, Q. Yang, L. Di, Y. Xing, G. Xie, C. Zhou, W. Wang, S. Chen, A stable Zn-MOF for photocatalytic Csp^3–H oxidation: vinyl double bonds boosting electron transfer and enhanced oxygen activation, ACS Catal. 12 (2022) 10668–10679, https://doi.org/10.1021/acscatal.2c02674.
[44] H. Li, W. Chen, Z. Yuan, Y. Jin, Y. Zhao, P. Ma, J. Niu, J. Wang, Controlled assembly of Ru-containing polyoxometalates for photocatalytic activity of the primary amine coupling reaction, Inorg. Chem. 61 (2022) 9935–9945, https://doi.org/10.1021/acs.inorgchem.2c00718.
[45] D. Liu, B. Chen, J. Li, Z. Lin, P. Li, N. Zhen, Y. Chi, C. Hu, Imidazole-functionalized polyoxometalate catalysts for the oxidation of 5-hydroxymethylfurfural to 2, 5-diformylfuran using atmospheric O_2, Inorg. Chem. 60 (2021) 3909–3916, https://doi.org/10.1021/acs.inorgchem.0c03698.
[46] A. Jana, J. Mondal, P. Borah, S. Mondal, A. Bhaumik, Y. Zhao, Ruthenium bipyridyl tethered porous organosilica: a versatile, durable and reusable heterogeneous photocatalyst, Chem. Commun. 51 (2015) 10746–10749, https://doi.org/10.1039/C5CC03067F.
[47] M. Zhang, Z. Yu, J. Xiong, R. Zhang, X. Liu, X. Lu, One-step hydrothermal synthesis of $Cd_xIn_yS_{(x+1.5y)}$ for photocatalytic oxidation of biomass-derived 5-hydroxymethylfurfural to 2, 5-diformylfuran under ambient conditions, Appl. Catal. B Environ. 300 (2022), 120738, https://doi.org/10.1016/j.apcatb.2021.120738.
[48] H.T. Abdel-Mohsen, J. Conrad, U. Beifuss, Laccase-catalyzed oxidation of hantzsch 1,4-dihydropyridines to pyridines and a new one pot synthesis of pyridines, Green Chem. 14 (2012) 2686–2690, https://doi.org/10.1039/C2GC35950B.
[49] S. Oudi, A.R. Oveisi, S. Daliran, M. Khajeh, R. Luque, U. Sen, H. García, Straightforward synthesis of a porous chromium-based porphyrinic metal-organic framework for visible-light triggered selective aerobic oxidation of benzyl alcohol to benzaldehyde, Appl. Catal. A Gen. 611 (2021), 117965, https://doi.org/10.1016/j.apcata.2020.117965.
[50] M. Safaiee, B. Ebrahimghasri, M.A. Zolfigol, S. Baghery, A. Khoshnood, D. A. Alonso, Synthesis and application of chitosan supported vanadium oxo in the synthesis of 1,4- dihydropyridines and 2,4,6-triarylpyridines via anomeric based oxidation, New J. Chem. 42 (2018) 12539–12548, https://doi.org/10.1039/C8NJ02062K.
[51] T. Toyao, N. Ueno, K. Miyahara, Y. Matsui, T.H. Kim, Y. Horiuchi, H. Ikeda, M. Matsuoka, Visible-light, photoredox catalyzed, oxidative hydroxylation of arylboronic acids using a metal-organic framework containing tetrakis (carboxyphenyl)porphyrin groups, Chem. Commun. 51 (2015) 16103–16106, https://doi.org/10.1039/C5CC06163F.